Applied Chemical Engineering (2026) Volume 9 Issue 3 ISSN: 2578-2010 (O)
doi: 10.59429/ace.v9i3.6059

ORIGINAL RESEARCH ARTICLE

Green synthesized Gracilaria folifera-mediated MgO-ZnO nanocomposite for photocatalytic and anticancer applications

M. Adhithi[1], M. Yogeswari[1,*], D.D. Padma Priya[2], S. Kannappan[3], K.Vinoth Kumar[4], N.J. Suthan Kissinger[5], B. Sangeetha[6], S. Sivakumar[7], B. Esther Bharathi[7]

[1] *Department of Physics, Vellalar College for Women (Autonomous), Erode 638012, Tamil Nadu, India*

[2] *Department of Mathematics-Applied Sciences, New Horizon College of Engineering, Bangalore 560103, Karnataka, India*

[3] *Department of Electronics and Communications Engineering, Siddharth Institute of Engineering & Technology, Puttur 517583, Andhra Pradesh, India*

[4] *Department of Electrical and Electronics Engineering, New Horizon College of Engineering, Bengaluru 560103, Karnataka, India*

[5] *Department of General Studies (Physics Section), Jubail Industrial College, Royal Commission for Jubail, P.O Box 35718, KSA*

[6] *Department of Electrical and Electronics Engineering, AVS Engineering College, Salem 636003, Tamilnadu, India*

[7] *Department of Physics, Government Arts College (Autonomous), Salem 636007, Tamilnadu, India*

***Corresponding author:** Yogeswari M, m.yogeswari@vcw.ac.in

ABSTRACT

Gracilaria folifera-mediated MgO-ZnO nanocomposite (GF-MgO-ZnO NC) was synthesized through a green approach utilizing G. folifera extract as a reducing, stabilizing, and biofunctionalizing agent. The structural, optical, photocatalytic, and anticancer properties of the synthesized nanocomposite were systematically investigated. X-ray diffraction analysis confirmed the coexistence of crystalline MgO and ZnO phases, indicating the successful formation of a mixed-oxide nanocomposite with good crystallinity. UV-Visible spectroscopy revealed broad absorption in the UV region and an optical band gap of 4.88 eV, suggesting electronic interactions between the MgO and ZnO components. The photocatalytic performance of GF-MgO-ZnO NC demonstrated effective degradation of methyl orange dye under UV irradiation, which may be associated with improved charge separation within the MgO-ZnO nanocomposite. The anticancer activity evaluated against HT29 colorectal cancer cells using the MTT assay exhibited a concentration-dependent reduction in cell viability, with an IC_{50} value of 93.23 µg/mL. The observed cytotoxicity may be associated with the synergistic effects of the MgO-ZnO nanocomposite and residual phytochemical species derived from G. folifera; however, the underlying molecular mechanisms were not directly investigated in the present study. These findings demonstrate that the green-synthesized GF-MgO-ZnO NC exhibits moderate photocatalytic activity and concentration-dependent cytotoxicity against HT29 colorectal cancer cells, warranting further investigation for environmental remediation and biomedical applications.

Keywords: green synthesis; *Gracilaria folifera*; MgO-ZnO nanocomposite; photocatalytic activity; cytotoxicity; HT29 cells; bandgap energy

ARTICLE INFO

Received: 8 June 2026
Accepted: 6 July 2026
Available online: 24 July 2026

1. Introduction

Nanostructured metal oxides have become indispensable in modern nanotechnology due to their tunable physicochemical characteristics, high surface activity, and broad applicability across

environmental and biomedical domains[1]. Among them, magnesium oxide (MgO) nanoparticles have garnered significant attention as a multifunctional material owing to their wide bandgap, strong ionic character, high thermal stability, and intrinsic ability to generate reactive oxygen species (ROS). At the nanoscale, MgO exhibits enhanced surface defects, increased electron mobility, and superior catalytic activity compared with its bulk counterpart, enabling efficient photocatalytic degradation of organic pollutants, antimicrobial performance, and promising anticancer effects[2]. Despite these advantages, pristine MgO often suffers from limitations such as narrow optical absorption, moderate charge transfer efficiency, and relatively slow electron-hole separation rates, all of which restrict its applicability in high-performance photocatalytic and biomedical systems[3].

One effective strategy to overcome these drawbacks is heteroatom incorporation, particularly using zinc oxide (ZnO), a direct bandgap semiconductor with well-known optoelectronic and photocatalytic capabilities[4]. The ionic radius of Zn^{2+} closely matches that of Mg^{2+}, enabling smooth lattice integration and the formation of MgO-ZnO mixed-oxide nanostructures without compromising crystallinity[5]. Equal-percentage ZnO doping introduces controlled lattice distortion, increases microstrain, and significantly enhances the density of oxygen vacancies-sites crucial for improving catalytic activity and facilitating efficient ROS generation[6]. The synergistic interaction between MgO and ZnO broadens the absorption profile, modifies electronic band alignment, promotes charge carrier separation, and enhances surface redox activity. As a result, ZnO-doped MgO systems exhibit higher photocatalytic efficiency and stronger oxidative stress-induced cytotoxicity against cancer cells when compared with undoped MgO[7].

Alongside the advancement in material design, the synthesis route plays a critical role in determining particle morphology, defect distribution, and biological compatibility. Conventional chemical synthesis approaches often rely on toxic reagents, high temperatures, and hazardous by-products, rendering them unsuitable for biomedical applications. Green synthesis, in contrast, offers an eco-friendly and sustainable alternative by utilizing bioactive molecules from plant or marine extracts to reduce metal ions and stabilize nanoparticles[8]. Marine macroalgae have become particularly attractive for this purpose due to their rich biochemical composition, including sulfated polysaccharides, polyphenols, proteins, flavonoids, terpenoids, and antioxidants. These naturally occurring compounds can act simultaneously as reducing, capping, and stabilizing agents, resulting in nanoparticles that possess enhanced colloidal stability and inherent biocompatibility[9]. Among red marine algae, *G. folifera* is especially noteworthy because of its high content of galactans, agar-forming compounds, sulfate groups, and antioxidative phytochemicals. These biomolecules not only facilitate controlled nucleation and growth of nanocrystals but also impart functional groups capable of modulating biological interactions.

The use of *G. folifera* during green synthesis may be beneficial for biomedical applications, as surface characteristics can influence nanoparticle-cell interactions and biological responses. The hybrid organic-inorganic interface formed during green synthesis enhances the solubility and stability of nanoparticles in physiological environments, and the attached phytochemicals can accelerate the induction of oxidative stress in cancer cells. Photocatalytic properties, typically explored in environmental studies, are also relevant for cancer therapy because photocatalytically generated ROS are capable of initiating mitochondrial dysfunction, DNA fragmentation, and apoptotic cell death. Colorectal cancer remains a major global health concern, and HT29 cells serve as a widely used human colorectal adenocarcinoma model for evaluating the cytotoxic potential of nanomaterials. Nanoparticles capable of simultaneously exhibiting strong photocatalytic activity and effective ROS-mediated anticancer effects therefore present a dual advantage in environmental and biomedical applications[10].

Recent advances in computational oncology and machine learning have opened new opportunities for accelerating the design of anticancer nanomaterials by correlating physicochemical characteristics with biological performance. Predictive models based on parameters such as particle size, surface chemistry,

bandgap, and ROS-generating capability may assist in identifying promising nanomaterials prior to experimental validation. Although the present work focuses on the experimental synthesis and evaluation of the G. folifera-mediated MgO-ZnO nanocomposite, integrating computational screening with experimental investigations represents a promising direction for the future development of nanotherapeutic materials.

Although MgO, ZnO, and MgO-ZnO nanocomposite have been extensively investigated, relatively few studies have reported the green synthesis of *G. folifera*-mediated MgO-ZnO nanocomposites with a comprehensive evaluation of their structural, optical, photocatalytic, and anticancer properties. Furthermore, the combined influence of ZnO incorporation and marine algal-assisted green synthesis on the physicochemical characteristics and multifunctional performance of MgO-ZnO nanocomposites has not been widely explored. Therefore, the present study aims to provide a systematic investigation of these properties using a *G. folifera*-mediated MgO-ZnO nanocomposite. There are relatively few reports that combine X-ray diffraction, UV-Visible spectroscopy, photocatalytic degradation analysis, scanning electron microscopy, energy-dispersive X-ray spectroscopy, and MTT cytotoxicity assessment within a single study of green-synthesized MgO-ZnO nanocomposites.

Beyond photocatalytic applications, green-synthesized MgO-based nanomaterials have attracted considerable attention for their antimicrobial, antibiofilm, antifungal, and anticancer activities owing to their surface reactivity and ROS-generating capability. The incorporation of ZnO and the use of marine algal extracts during green synthesis can further enhance the multifunctional nature of these materials by influencing their surface characteristics and biological interactions. Such multifunctional oxide nanoplatforms offer opportunities for both environmental remediation and biomedical applications. A comparative summary of algae-mediated metal oxide and metal oxide nanocomposites reported in the literature, including their structural, optical, photocatalytic, and anticancer properties, is presented in **Table 1** to highlight the significance and research gap addressed by the present GF-MgO-ZnO nanocomposite.

Table 1. Comparison of algae-mediated metal oxide and metal oxide nanocomposites reported in the literature with the present GF-MgO-ZnO NC.

Ref. No.	Synthesis Route / Algal Source	Material	Particle Size (nm)	Bandgap (eV)	Photocatalytic Performance	Anticancer Performance
[11]	*Gracilaria edulis* (green synthesis)	ZnO nanoparticles	18-42	3.20-3.30	Not reported	Antioxidant activity reported
[12]	Algal biomass (phyco-synthesis)	Ag-ZnO nanocomposite	10-50	2.90-3.15	Not reported	Biomedical activity reported
[13]	Brown seaweed extract (green synthesis)	ZnO-Fe_2O_3 nanocomposite	25-60	2.10-2.80	Dye removal reported	Not reported
[14]	Marine algal extract (eco-friendly synthesis)	TiO_2-ZnO nanocomposite	20-55	2.90-3.20	reported	Not reported
[15]	Seaweed extract	MgO nanoparticles	30-80	4.80-5.20	Catalytic activity reported	Not reported
Present Work	*G. folifera* (green-assisted synthesis)	GF-MgO-ZnO NC	24-47	4.88	Moderate methyl orange degradation (26.61%) under UV irradiation	IC_{50} = 93.23 µg/mL against HT29 cells

In this context, the present work aims to synthesize a *G. folifera*-mediated MgO-ZnO nanocomposite through a green synthetic route and to evaluate its physicochemical and biological properties. The bioactive constituents present in the algal extract serve as natural reducing and stabilizing agents during nanocomposite formation. The synthesized material was systematically characterized to investigate the influence of ZnO incorporation and algal-assisted green synthesis on its structural and optical properties. Its photocatalytic performance was evaluated through the degradation of methyl orange under UV irradiation, while its anticancer activity was assessed against HT29 colorectal cancer cells using the MTT assay. Through this comprehensive investigation, the study provides insights into the role of ZnO incorporation and marine algal-assisted synthesis in tailoring the multifunctional properties of MgO-based nanomaterials and demonstrates their potential for environmental remediation and further biomedical investigations.

2. Experimental Methods and Materials Used

Fresh specimens of the red macroalga *G. folifera* were collected from the Gulf of Mannar region and thoroughly washed with seawater followed by repeated rinsing with distilled water to remove salt, sand, and epiphytic contaminants[16]. The washed seaweed was shade-dried, finely powdered using a mechanical grinder, and stored in an airtight container until further use. Magnesium nitrate hexahydrate [$Mg(NO_3)_2 \cdot 6H_2O$, 98%] and zinc nitrate hexahydrate [$Zn(NO_3)_2 \cdot 6H_2O$, 98%] were procured from NICE Chemicals Pvt. Ltd., India, and utilized without further purification. Double-distilled water served as the solvent throughout the synthetic procedure, while ethanol was employed to wash the final product to ensure the removal of residual organics.

To prepare the *G. folifera* extract, 2 g of dried and powdered seaweed was mixed with 100 mL of distilled water and heated at 60 °C for 1 hour under continuous stirring at 720 rpm. During this process, bioactive compounds such as sulfated polysaccharides, phenolics, and proteins were released into the aqueous medium. The heated mixture was subsequently allowed to cool and filtered using Whatman No. 1 filter paper to obtain a clear phytochemical-rich extract, which served as the natural reducing, stabilizing, and fuel source for nanoparticle formation[17].

For the synthesis of equimolar ZnO-doped MgO nanoparticles, 0.25 M $Mg(NO_3)_2 \cdot 6H_2O$ and 0.25 M $Zn(NO_3)_2 \cdot 6H_2O$ were dissolved together in 40 mL of freshly prepared *G. folifera* extract. The resulting precursor mixture was magnetically stirred at 60 °C for 1 hour to promote metal-ion chelation by algal phytochemicals[18]. This was followed by ultrasonication for 30 minutes to ensure homogeneous dispersion of ions and enhance nucleation kinetics. The sol obtained after ultrasonication was allowed to undergo further stirring and then left to age overnight to enable the formation of a stable gel network[19]. The gel was filtered and thoroughly washed with distilled water and ethanol to remove unbound organic residues and nitrate impurities.

The washed gel was dried overnight at 150 °C in a hot-air oven, resulting in a solid precursor mass. The dried material was then subjected to calcination at 400 °C for 3 hours in a muffle furnace to decompose residual organic matter, remove moisture, and transform the precursor into crystalline equimolar ZnO-doped MgO nanoparticles. The final product obtained after calcination represented the GF-MgO-ZnO nanocomposite synthesized through a green, algal-assisted route, as illustrated in **Figure 1**[20].

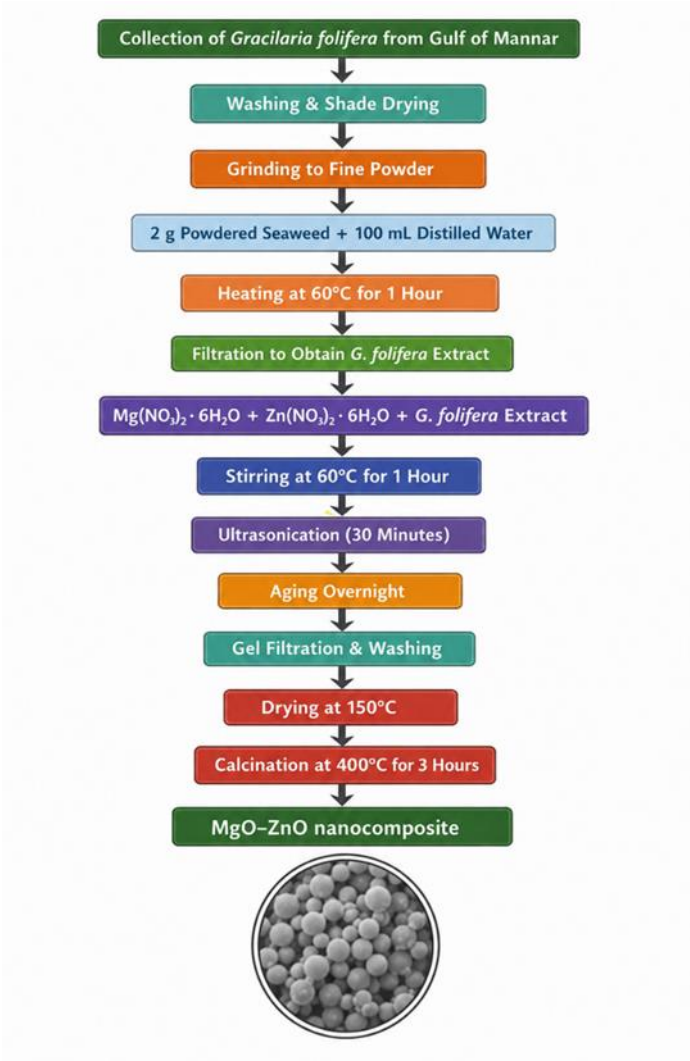

Figure 1. Schematic representation of the green synthesis route for equimolar GF-MgO-ZnO nanocomposite.

3. Characterization Techniques

The crystalline structure of MgO-*G. folifera* and equimolar GF-MgO-ZnO nanocomposite was analyzed using X-ray diffraction (XRD) on a Bruker D2 Phaserdiffractometer equipped with Cu Kα radiation (λ = 1.5406 Å), operated at 40 kV and 30 mA, over a 2θ range of 20°-80°. Fourier Transform Infrared (FTIR) spectra were recorded using a PerkinElmer Spectrum FTIR spectrometer in the range of 4000-400 cm^{-1} (KBr pellet method) to identify metal oxygen bonding and biofunctional groups originating from *G. folifera* phytochemicals. Optical absorption properties were examined using a UV-Visible spectrophotometer in the wavelength range of 200-800 nm, and the optical bandgap energy was determined using Tauc plots assuming direct allowed transitions. The photocatalytic activity of the synthesized nanocomposite was evaluated through the degradation of methyl orange under UV irradiation, and the degradation efficiency was monitored using UV-Visible spectroscopy. Anticancer activity was assessed by MTT cytotoxicity assay against HT29 human colorectal cancer cells, and the cell viability was measured at 570 nm using a microplate reader.

3.1. X-ray Diffraction (XRD) Analysis

The X-ray diffraction (XRD) patterns of the green-synthesized MgO-*G. folifera* and GF-MgO-ZnO NC are presented in **Figure 2**. The diffraction pattern of MgO-*G. folifera* exhibits distinct reflections at 2θ values of 36.88°, 42.85°, 62.20°, and 74.57°, corresponding to the (111), (200), (220), and (311) crystallographic planes, respectively. These diffraction peaks are in good agreement with the standard cubic periclase phase of

MgO (JCPDS Card No. 45-0946), confirming the successful formation of crystalline MgO nanoparticles. The absence of additional diffraction peaks indicates the high phase purity of the synthesized material[21].

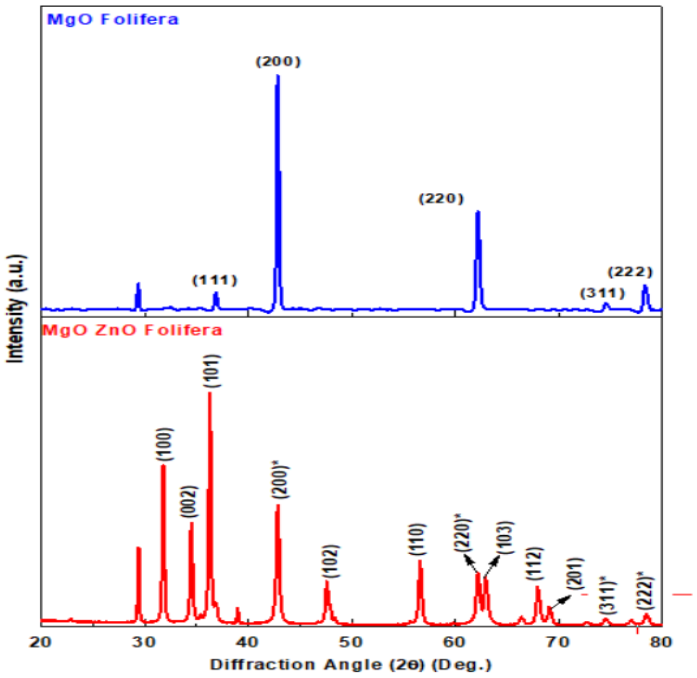

Figure 2. X-ray diffraction patterns of MgO-*G. folifera* and GF-MgO-ZnO NC.

The XRD pattern of the GF-MgO-ZnO NC exhibits characteristic reflections at 2θ values of 31.79°, 34.50°, 36.29°, 42.85°, and 47.68°, which are indexed to the (100), (002), (101), (102), and (111) crystallographic planes, respectively. These reflections are consistent with the hexagonal wurtzite structure of ZnO and match well with JCPDS Card No. 36-1451. The presence of diffraction peaks associated with both MgO and ZnO phases confirms the successful formation of the MgO-ZnO nanocomposite through the green synthesis route. No significant impurity peaks corresponding to secondary crystalline phases were observed, indicating the purity of the synthesized nanocomposite.

The relatively broad diffraction peaks observed for both samples indicate their nanocrystalline nature. The average crystallite size was estimated using the Debye-Scherrer equation, and the calculated values are summarized in **Table 2**. The average crystallite size of MgO-*G. folifera* was found to be 34.75 nm, whereas the GF-MgO-ZnO NC exhibited an average crystallite size of 33.40 nm. The slight reduction in crystallite size following the incorporation of ZnO suggests a marginal influence on crystal growth during nanocomposite formation. Such variations may arise from differences in nucleation and growth kinetics during the synthesis process[22]. The observed peak broadening and crystallite size variations provide qualitative evidence of microstructural changes; however, the specific nature of any associated defect states was not directly investigated in the present study.

Table 2. X-ray diffraction (XRD) parameters showing diffraction angle (2θ), Miller indices (hkl), and Scherrer crystallite size.

Sample	2θ (°)	(hkl)	Crystallite size (nm)
MgO-G. *folifera*	36.88	(111)	42
	42.85	(200)	33
	62.20	(220)	36
	74.57	(311)	28
GF-MgO-ZnO NC	31.79	(100)	47
	34.50	(002)	34
	36.29	(101)	30
	42.85	(102)	32
	47.68	(111)	24

The coexistence of crystalline MgO and ZnO phases demonstrates the successful fabrication of a mixed-oxide nanocomposite. The formation of interfaces between MgO and ZnO phases may contribute to the functional properties of the material by modifying its microstructural characteristics. Overall, the XRD results confirm the formation of highly crystalline MgO and ZnO phases and establish the successful synthesis of an MgO-ZnO nanocomposite with nanocrystalline dimensions and good phase purity through a green synthesis approach employing *G. folifera* extract.

3.2. FTIR analysis

The FTIR spectrum of the calcined G.F-MgO-ZnO NC (**Figure 3**) exhibits characteristic absorption bands corresponding predominantly to the inorganic oxide framework, together with weak bands arising from residual surface functionalities associated with the green synthesis using *G.folifera*. The comparatively weak intensity of the organic absorption bands indicates that most phytochemical constituents of the algal extract were decomposed during calcination, while minor surface functionalities may still remain on the nanocomposite surface.

The broad absorption bands observed at 3738 and 3454 cm^{-1} are assigned to O-H stretching vibrations of surface hydroxyl groups and adsorbed water molecules. These hydroxyl groups are commonly observed on metal oxide surfaces and may originate from surface hydration as well as residual oxygen-containing species associated with the *G. folifera*-mediated synthesis.

A weak absorption band at 2307 cm^{-1} is attributed to the asymmetric stretching vibration of adsorbed atmospheric CO_2. Such bands are frequently observed in oxide nanomaterials because of the interaction between basic oxide surfaces and carbon dioxide from the atmosphere.

The absorption bands located at 1759 and 1693 cm^{-1} are assigned to C=O stretching vibrations of carbonyl-containing species. These bands may arise from trace oxygenated organic residues derived from the *G. folifera* extract or from surface carbonate-related species formed during sample exposure to air. Their relatively low intensity indicates that only a small amount of such surface species remains after calcination.

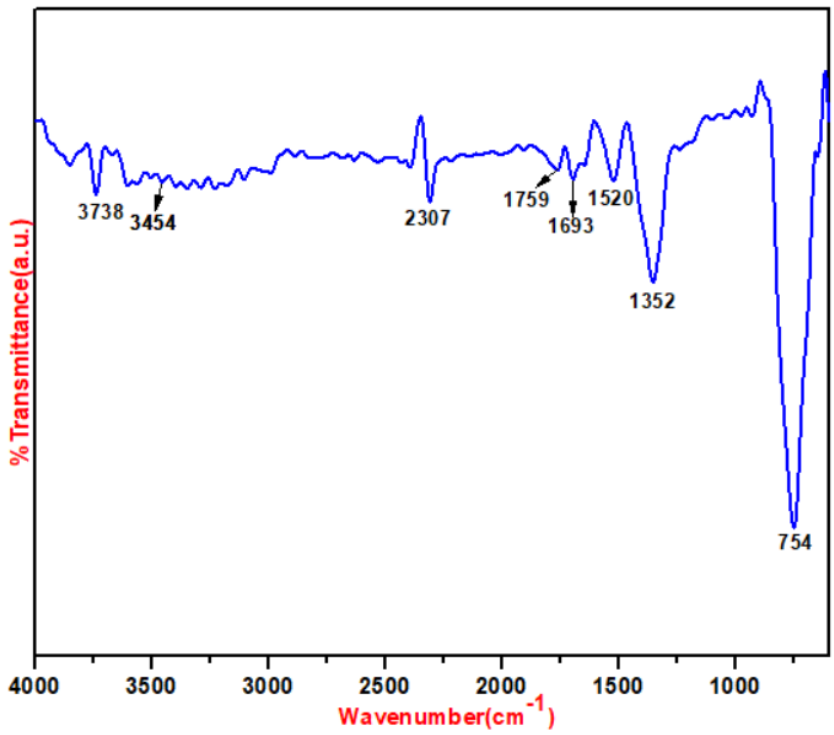

Figure 3. FTIR spectrum of GF-MgO-ZnO NC.

The band observed at 1520 cm^{-1} may be attributed to asymmetric stretching vibrations of surface carbonate species or residual organic functional groups, whereas the absorption at 1352 cm^{-1} is associated with C-O stretching and/or carbonate-related vibrations. These bands suggest the possible presence of minor surface oxygen-containing species, which are commonly reported for green-synthesized metal oxide nanomaterials.

The intense absorption band centred at 754 cm^{-1} is assigned to the stretching vibrations of metal-oxygen (M-O) bonds arising from the Mg-O and Zn-O lattice. This dominant band confirms the successful formation of the MgO-ZnO nanocomposite. The broad nature of the metal-oxygen absorption is consistent with the coexistence of MgO and ZnO phases within the nanocomposite, as observed in the XRD analysis.

Overall, the FTIR results indicate that the synthesized G.F-MgO-ZnO NC consists predominantly of an inorganic MgO-ZnO framework with characteristic metal-oxygen bonding. The weak residual organic bands suggest that *G. folifera* primarily served as a natural reducing and stabilizing agent during the green synthesis process, while only minor surface functionalities may remain after calcination. These surface groups may contribute to the surface characteristics of the nanocomposite without significantly altering its crystalline oxide framework.

3.3. UV-Visible Absorption Analysis

The UV-Visible absorption spectrum of the GF-MgO-ZnO NC presented in **Figure 4** displays a dominant and broad absorption band in the deep-UV region, extending prominently from approximately 180 to 360 nm, which is characteristic of wide-bandgap oxide semiconductors. The intense absorption maxima observed in the 180-240 nm range, along with the presence of double-peaked shoulders, signify the convolution of multiple intrinsic and defect-mediated electronic transitions within the mixed MgO-ZnO lattice. The absorption intensity exceeding 1.0 absorbance units indicates strong photon-matter interactions, reflecting the high density of electronic states and optical transition pathways generated through the synergistic contributions of the semiconductor matrix and defect-induced energy levels[25].

The steep rise in absorbance below 250 nm corresponds primarily to intrinsic excitonic transitions involving $O^{2-} \rightarrow$ metal (Mg^{2+}/Zn^{2+}) charge transfer processes. While MgO exhibits excitonic features in the far-UV region due to its ultra-wide bandgap (~7.8 eV), ZnO absorbs closer to 360 nm owing to its 3.37 eV bandgap. The intermediate spectral distribution observed in **Figure 4** confirms the successful formation of a MgO-ZnO mixed-oxide lattice, where the electronic transitions of both components overlap, hybridize, and create a broadened absorption envelope. The shoulder-like features and local fluctuations in the 180-240 nm region are attributed to transitions involving lattice defects such as oxygen vacancies (V_0), Mg/Zn interstitials, and F-center states. These defects introduce donor-like mid-gap energy levels that contribute to band tailing and effectively shift the absorption edge to longer wavelengths[26].

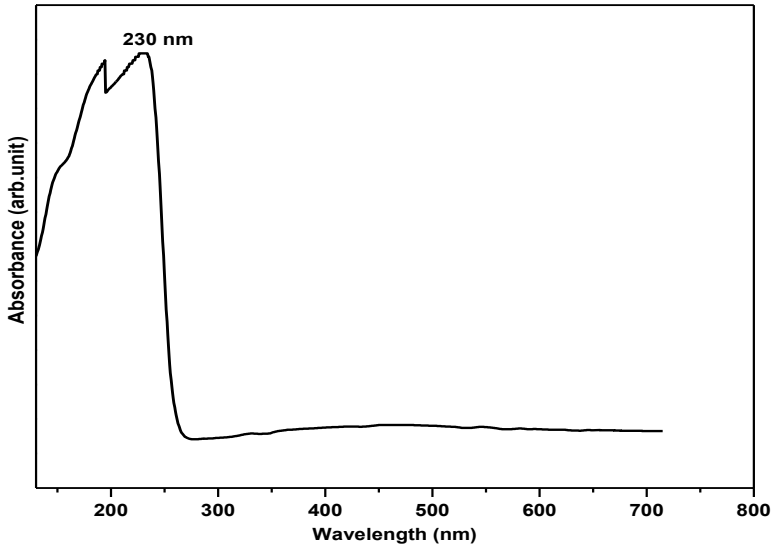

Figure 4. UV-Visible absorption spectrum of G.F-MgO-ZnO NC.

Furthermore, *G. folifera*-assisted synthesis introduces bio-organic ligands, including sulfated polysaccharides, phenolic groups, and carbonyl functionalities, which interact transiently with Mg^{2+} and Zn^{2+} ions during nanoparticle nucleation. These interactions give rise to ligand-to-metal charge transfer (LMCT) transitions, which contribute to the minor spectral oscillations and broadened profile recorded in the UV region. Although the majority of these functional groups are decomposed during calcination, a small fraction remains chemisorbed on the nanoparticle surface, modifying the surface electronic potential and introducing additional optical response features.

The sharp intensity drop above 260-280 nm, as seen in **Figure 4**, marks the point at which the material ceases to absorb photons in the visible region, consistent with its wide-bandgap semiconductor nature. Beyond 400 nm, the absorption curve becomes nearly flat and slightly negative due to baseline correction and negligible optical response, confirming the UV-specific absorption of the material. This behavior is typical of defect-modified wide-bandgap photocatalysts, ensuring that photon-induced charge excitation is highly efficient under UV illumination where photon energy exceeds the bandgap threshold.

Collectively, the absorption profile in **Figure 4** validates three critical optical attributes of the nanocomposite: (1) strong UV absorption arising from intrinsic wide-bandgap transitions; (2) defect-induced shoulders associated with ZnO incorporation and *G. folifera*-mediated synthesis and (3) a clearly defined absorption edge reflecting the formation of an electronically coupled MgO-ZnO mixed-oxide system. These features confirm the suitability of the material for UV-driven photocatalysis and ROS-mediated applications.

3.4. Bandgap Energy Analysis

The optical bandgap of the GF-MgO-ZnO NC was evaluated from the Tauc plot shown in **Figure 5**, where $(\alpha h\nu)^2$ is plotted as a function of photon energy ($h\nu$) assuming a direct allowed transition. The absorption coefficient α was obtained from the UV-Vis data using the relation $\alpha=2.303A/t$, where A is the absorbance and t is the optical path length. For direct bandgap semiconductors, the Tauc relation $(\alpha h\nu)^2=A(h\nu - E_g)$ predicts that the linear portion of the $(\alpha h\nu)^2$ versus $h\nu$ curve, when extrapolated to intersect the energy axis, yields the optical bandgap E_g. In **Figure 5**, a well-defined linear region is observed in the high-energy side of the curve, and extrapolation of this segment to $(\alpha h\nu)^2=0$ gives an E_g value of 4.88 eV. This bandgap lies intermediate between the values reported for bulk MgO (~7.8 eV) and bulk ZnO (~3.37 eV), suggesting electronic interaction between the MgO and ZnO phases within the nanocomposite[27].

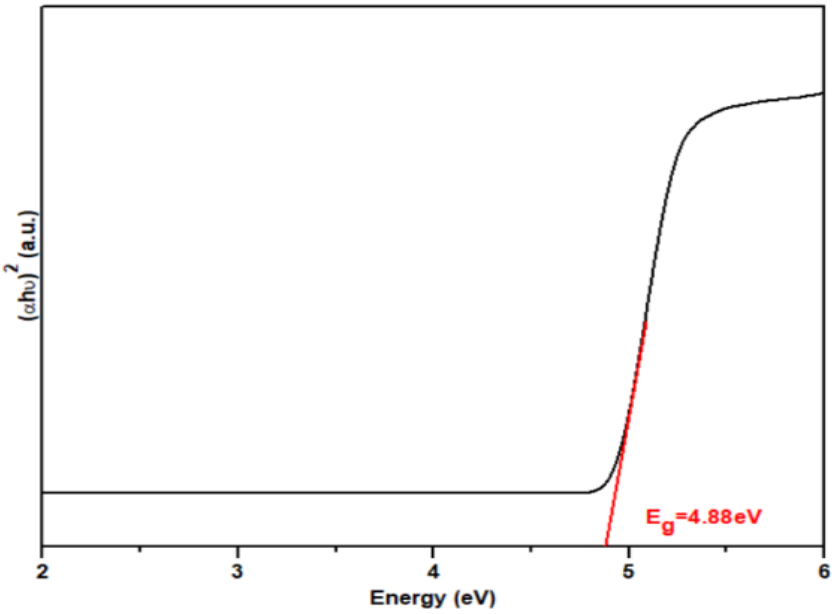

Figure 5. Tauc plot $(\alpha h\nu)^2$versus photon energy for GF-MgO-ZnO NC.

The reduction in the optical bandgap relative to pristine MgO may be attributed to the synergistic interaction between the MgO and ZnO phases within the nanocomposite. ZnO incorporation may introduce lattice strain and possible defect-related states that influence the electronic structure and facilitate optical transitions at lower energies. In addition, the *G. folifera*-mediated green synthesis may modify the surface electronic environment through residual surface functionalities, which could also contribute to the observed shift in the absorption edge[28]. Thus, the observed bandgap of 4.88 eV suggests electronic interaction between the MgO and ZnO phases within the green-synthesized nanocomposite. The modified optical properties may contribute to the UV photoresponse and photocatalytic behaviour of the synthesized material.

3.5. Photocatalytic Degradation Behaviour

The photocatalytic degradation behaviour of the GF-MgO-ZnO NC was investigated using methyl orange (MO) as a model organic dye under UV irradiation, and the corresponding spectral evolution is presented in **Figure 6(a)**. A gradual decrease in absorbance intensity was observed with increasing irradiation time, indicating the progressive degradation of MO in the presence of the synthesized nanocomposite. The absorption band located in the UV region decreased systematically from the initial irradiation stage to 100 min, confirming a reduction in dye concentration during the photocatalytic process[29,30].

The initial absorbance of MO decreased from 1.06294 to 0.78010 after 100 min of UV exposure. The degradation efficiency was calculated using:

$$Degradation\ (\%) = \frac{C_0 - C_t}{C_0} \times 100$$

where C_0 and C_t represent the initial concentration and concentration at irradiation time t, respectively.

The calculated degradation efficiency was found to be 26.61% after 100 min of irradiation, demonstrating moderate photocatalytic activity of the *G. folifera*-derived MgO-ZnO nanocomposite toward methyl orange degradation.

To evaluate the degradation kinetics, the experimental data were fitted using the pseudo-first-order kinetic model:

$$\ln\left(\frac{C_t}{C_0}\right) = -kt$$

where k is the apparent first-order rate constant and t is the irradiation time. The kinetic plot shown in **Figure 6(b)** exhibits an excellent linear relationship between $\ln(C_0/C_t)$ and irradiation time, indicating that the degradation process follows pseudo-first-order kinetics. The calculated rate constant was 3.10×10^{-3} min^{-1} with a correlation coefficient (R^2) of approximately 0.999, confirming good agreement between the experimental data and the kinetic model.

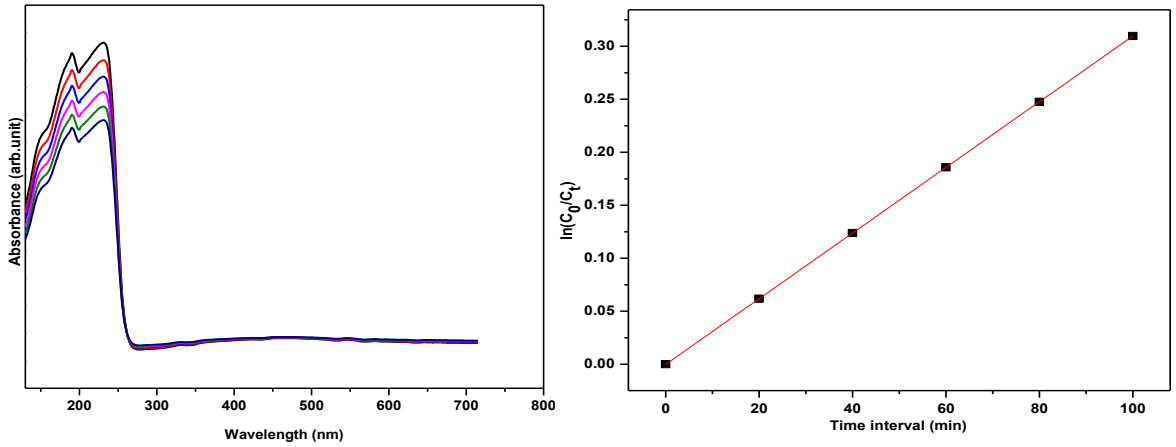

Figure 6. (a) UV-Visible spectral evolution during the photocatalytic degradation of methyl orange using the G.F-MgO-ZnO NC under UV irradiation and (b) corresponding pseudo-first-order kinetic plot (ln (C_0/C_t)) for methyl orange degradation.

The observed photocatalytic activity may be associated with the coexistence of MgO and ZnO phases within the nanocomposite. The presence of both oxide phases could influence interfacial interactions and charge-transfer behaviour under UV irradiation. In addition, the green synthesis route employing *G. folifera* extract may contribute to the formation of a surface environment favorable for dye adsorption and photocatalytic interaction.

Although no ZnO_2 phase was detected in the present *G. folifera*-mediated MgO-ZnO nanocomposite, oxygen-rich zinc-based materials such as ZnO_2 have been reported to enhance ROS generation and redox activity. This highlights the broader importance of Zn-containing oxide systems in photocatalytic and biomedical applications and may provide a useful direction for future studies.

Table 3. Comparison of the photocatalytic degradation performance of the present GF-MgO-ZnO NC with previously reported MgO-, ZnO-, and MgO-ZnO-based photocatalysts for methyl orange degradation.

Photocatalyst	Synthesis Route	Pollutant	Irradiation Time	Degradation Efficiency (%)	Remarks	Ref.
Green-synthesized MgO nanoparticles	Plant-mediated	Methyl Orange	120 min	95	High activity attributed to high surface area	[31]
Pullulan-mediated porous ZnO microflowers	Green synthesis	Methyl Orange	120 min	~92	Porous morphology enhanced degradation	[32]
ZnO photocatalyst	Chemical synthesis	Methyl Orange	320 min	73.56	Pure ZnO showed moderate activity	[33]
Mn_3O_4@ZnO hybrid nanocomposite	Hydrothermal	Methyl Orange	240 min	89.99	Heterojunction improved charge separation	[33]
Sn-ZnO/GO nanocomposite	Sol-gel	Methyl Orange	120 min	96.2	Graphene oxide enhanced electron transport	[34]
Present work (GF-MgO-ZnO NC)	*G. folifera*-mediated green synthesis	Methyl Orange	100 min	26.61	Moderate photocatalytic activity under UV irradiation	Present work

The photocatalytic performance of the present GF-MgO-ZnO NC was compared with previously reported MgO-, ZnO-, and MgO-ZnO-based photocatalysts, as summarized in **Table 3**. The present nanocomposite exhibited a degradation efficiency of 26.61% after 100 min of UV irradiation, which is lower than that reported for several optimized photocatalysts. This moderate performance may be attributed to differences in synthesis conditions, catalyst composition, and experimental parameters. Furthermore, the primary objective of the present study was to synthesize and investigate the structural, optical, photocatalytic, and anticancer properties of the *G. folifera*-mediated MgO-ZnO nanocomposite rather than to optimize photocatalytic degradation efficiency. The irradiation wavelength and intensity of the UV light source were not recorded during the present study and will be carefully documented in future investigations to facilitate reproducibility.

Overall, the results indicate that the *G. folifera*-mediated MgO-ZnO nanocomposite exhibits measurable photocatalytic activity toward methyl orange degradation under UV irradiation. The progressive decrease in absorbance intensity together with the pseudo-first-order kinetic behaviour demonstrates the photocatalytic activity of the synthesized *G. folifera*-mediated MgO-ZnO nanocomposite under UV irradiation.

3.6. Anti-cancer Activity

The antiproliferative activity of MgO-*G. folifera* and G.F-MgO-ZnO-NC against HT29 human colorectal carcinoma cells was evaluated using a concentration-dependent MTT assay, and the corresponding morphological changes were examined microscopically. The cytotoxicity profile of the G.F-MgO-ZnO-NC sample, presented in **Figure 7**, demonstrates a concentration-dependent reduction in cell viability, indicating its inhibitory effect on HT29 cell proliferation[35].

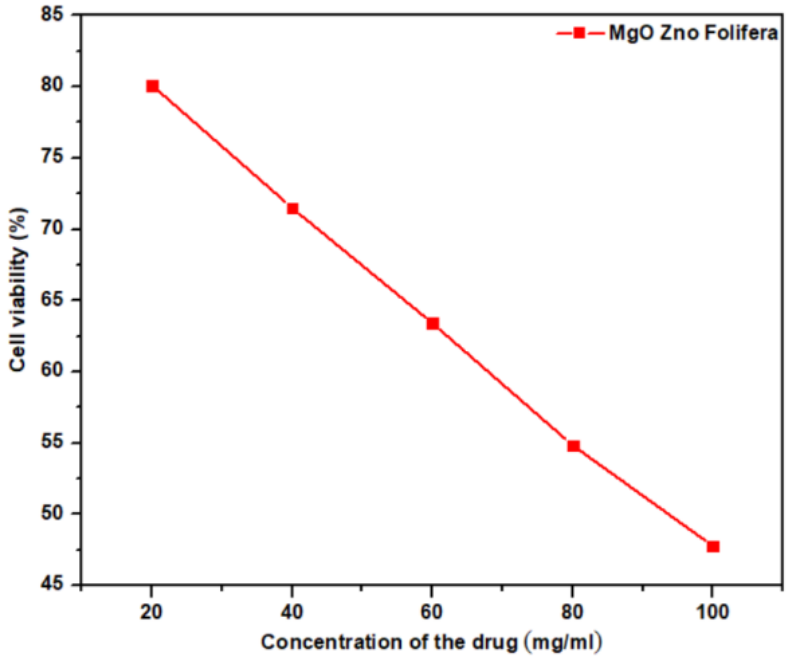

Figure 7. Plotting of concentration of drugs Vs Cancer cell viability percentage.

At the lowest tested concentration of 20 µg/mL, cell viability remained at approximately 80%, suggesting limited cytotoxicity. As the concentration increased to 40 µg/mL, viability decreased to approximately 71%, indicating the onset of a measurable antiproliferative response. A further decrease in viability was observed at 60 µg/mL (~63%) and 80 µg/mL (~55%), demonstrating a progressive reduction in cellular metabolic activity with increasing nanoparticle concentration. At the highest tested concentration of 100 µg/mL, cell viability decreased to approximately 48%, indicating significant cytotoxicity toward HT29 cells.

The quantitative inhibition data and the corresponding IC_{50} value of 93.23 µg/mL, summarized in Table 3, indicate moderate cytotoxic activity of the G.F-MgO-ZnO-NC sample within the investigated concentration range. The gradual decrease in cell viability with increasing concentration suggests a concentration-dependent cytotoxic response. **Table 4** summarizes the percentage cell viability of HT29 cells following treatment with different concentrations of the nanocomposite.

Table 4. Proliferation activity of different concentration of HT29 colorectal cancer cell line of G.F-MgO-ZnO-NC with and its IC_{50} value.

Concentration (µg/mL)	Inhibition by G.F-MgO-ZnO-NC (%)	IC_{50} value (µg/mL)
20	80.09	
40	71.50	
60	63.40	93.23
80	54.83	
100	47.76	

The enhanced cytotoxic activity observed for the MgO-ZnO nanocomposite compared with MgO may be associated with the synergistic interaction between the MgO and ZnO phases. Previous studies have reported that MgO- and ZnO-based nanomaterials can influence cellular viability through oxidative stress-related pathways and nanoparticle-cell interactions. However, the underlying molecular mechanisms, including ROS generation and apoptosis-related processes, were not directly investigated in the present study and therefore cannot be conclusively established[36].

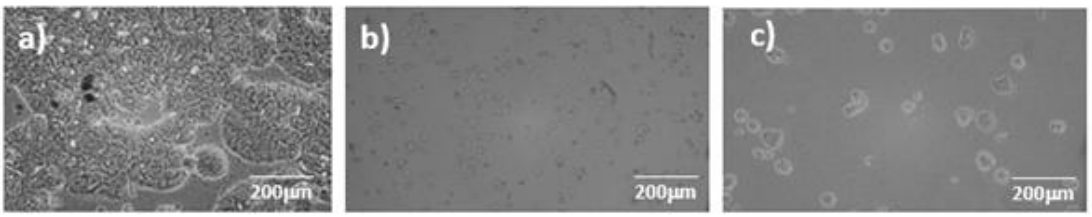

Figure 8. Morphology changes of Control (a), Etoposide treated cell (b) G.F-MgO-ZnO NC treated cell (c).

Residual phytochemical species derived from *G. folifera* may contribute to the surface characteristics and dispersion behaviour of the nanocomposite. Such surface modifications may influence nanoparticle-cell interactions and cellular uptake, thereby contributing to the observed biological response. However, detailed mechanistic investigations of intracellular pathways were beyond the scope of the present work.

The morphological observations shown in **Figure 8** support the MTT assay results. Untreated control HT29 cells (**Figure 8a**) exhibited normal epithelial morphology with dense cellular distribution and intact cellular structure. In contrast, cells treated with the standard anticancer drug etoposide (**Figure 8b**) showed a marked reduction in cell density and noticeable morphological alterations. Similarly, HT29 cells treated with the G.F-MgO-ZnO-NC sample (**Figure 8c**) exhibited cell shrinkage, loss of adhesion, and reduced cell density, indicating a cytotoxic response. However, the specific mode of cell death could not be determined from morphological observations alone.

Although the present study focused on in vitro cytotoxicity against HT29 cells, the ROS-active MgO-ZnO nanocomposite may provide a useful platform for future multifunctional therapeutic approaches. Integration with photoresponsive, photothermal, or externally assisted treatment strategies could further enhance anticancer efficacy and warrants future investigation.

Overall, the results obtained from **Figure 7**, **Figure 8**, and **Table 3** demonstrate a concentration-dependent reduction in HT29 cell viability following treatment with the G.F-MgO-ZnO-NC sample. The observed cytotoxicity may be associated with mechanisms previously reported for MgO- and ZnO-based nanomaterials; however, direct mechanistic evidence was not obtained in the present study. Furthermore, only HT29 cancer cells were evaluated, and therefore the selectivity and cytocompatibility of the nanocomposite toward normal cells remain to be established through future investigations.

4. Conclusion

In this study, a GF-MgO-ZnO NC was successfully synthesized through an environmentally friendly green synthesis approach using *G folifera* extract. Structural characterization confirmed the formation of crystalline MgO and ZnO phases within the nanocomposite, while optical analysis revealed an intermediate optical bandgap of 4.88 eV, indicating that ZnO incorporation influenced the optical properties of the MgO-based material. The synthesized GF-MgO-ZnO NC exhibited moderate photocatalytic activity toward methyl orange degradation under UV irradiation, achieving a degradation efficiency of 26.61% and following pseudo-first-order reaction kinetics. The nanocomposite also demonstrated concentration-dependent cytotoxicity against HT29 colorectal cancer cells, with an IC_{50} value of 93.23 µg/mL, accompanied by noticeable morphological changes in treated cells. Although the observed photocatalytic and anticancer activities may be associated with mechanisms reported for MgO- and ZnO-based nanomaterials, the underlying molecular pathways were not directly investigated in the present study. Furthermore, only HT29 cancer cells were evaluated; therefore, additional studies involving normal cell lines and detailed mechanistic investigations are required to establish the selectivity, biosafety, and mode of action of the nanocomposite. Overall, the findings demonstrate that the GF-MgO-ZnO NC synthesized using *G. folifera* extract exhibits measurable

photocatalytic activity and concentration-dependent anticancer effects, highlighting its potential for environmental remediation and serving as a promising candidate for further biomedical investigation.

Author contributions statement

Conceptualization, M. Adhithi, M. Yogeswari; Methodology, M. Yogeswari, D.D.Padma Priya; Investigation, M. Yogeswari, D.D. Padma Priya; Resources, S. Kannappan, K. Vinoth Kumar, N.J. Suthan Kissinger, B. Sangeetha; Writing, M. Adhithi, S. Sivakumar, B. Esther Bharathi. All authors have read and agreed to the published version of the manuscript.

Funding statement

The authors received no specific funding for this study.

Acknowledgments

Nil

Conflicts of interest

The authors declare that they have no conflicts of interest to report regarding the present study.

References

1. Soliman, M.K., Talib, A.H., Mahmoud, R., Ali, Z.A., Al-Haideri, H.H., Abalkhail, A., Binshaya, A.S., Salem, M.H., Al-Otibi, F.O. and Yassin, M.T., 2025. Ecofriendly magnesium oxide nanoparticles: anticancer, antimicrobial, and antidiabetic potentials in vitro. AMB Express, 15(1), p.143.
2. Ahamed, M., Akhtar, M.J. and Khan, M.M., 2023. Green-fabricated MgO nanoparticles: A potent antimicrobial and anticancer agent. Journal of King Saud University-Science, 35(8), p.102889.
3. Arif, T., Manzoor, S., Hussain, S., Younas, S., Jahangir, G.Z., Saleem, M.Z. and Hussain, N., 2026. Neem-mediated green synthesis of zinc oxide nanoparticles: therapeutic mechanisms, environmental utility, and critical research frontiers. Journal of Life and Social Sciences, 2026(1), pp.51-51.
4. Gatou, M.A., Bovali, N., Lagopati, N. and Pavlatou, E.A., 2024. MgO nanoparticles as a promising photocatalyst towards rhodamine B and rhodamine 6G degradation. Molecules, 29(18), p.4299.
5. Al-Harbi, L.M., Ezzeldien, M., Elhenawy, A.A. and Said, A.H., 2024. Assessment of the bioactivity of bioinspired magnesium oxide nanoparticles from the Azadirachta indica extract. Frontiers in Bioengineering and Biotechnology, 12, p.1480694.
6. Bhoi, H., Tiwari, S., Lal, G., Jani, K.K., Modi, S.K., Seal, P., Saharan, V., Modi, K.B., Borah, J.P., Punia, K. and Kumar, S., 2022. Green synthesis and characterization of Mg0. 93Na0. 07O nanoparticles for antimicrobial activity, cytotoxicity and magnetic hyperthermia. Ceramics International, 48(19), pp.28355-28373.
7. Daniele, V., Volpe, A.R., Cesare, P. and Taglieri, G., 2023. MgO Nanoparticles Obtained from an Innovative and Sustainable Route and Their Applications in Cancer Therapy. Nanomaterials 2023, 13, 2975 [online].
8. Swathi Pon Sakthi Sri, V., Aron Santhosh Kumar, Y., Savurirajan, M., Jha, D.K., Vinithkumar, N.V. and Dharani, G., 2024. Anticancer efficacy of magnetite nanoparticles synthesized using aqueous extract of brown seaweed Rosenvingea intricata, South Andaman, India. Scientific Reports, 14(1), p.20255.
9. Alprol AE, Mansour AT, El-Beltagi HS, Ashour M. Algal extracts for green synthesis of zinc oxide nanoparticles: promising approach for algae bioremediation. Materials 2023;16:2819.
10. Zeytünlüoğlu, A., 2024. Green synthesized seaweeds-based metal nanoparticles: therapeutic prospective for anticancer activity. International Journal of Chemistry and Technology, 8(2), pp.10-19.
11. Subramanian, H., Krishnan, M. and Mahalingam, A., 2022. Photocatalytic dye degradation and photoexcited anti-microbial activities of green zinc oxide nanoparticles synthesized via Sargassum muticum extracts. RSC advances, 12(2), pp.985-997.
12. Alprol, A.E., Mansour, A.T., Abdelwahab, A.M. and Ashour, M., 2023. Advances in green synthesis of metal oxide nanoparticles by marine algae for wastewater treatment by adsorption and photocatalysis techniques. Catalysts, 13(5), p.888.
13. Chaudhary, S. and Bharadvaja, N., 2023. Recent developments in phycosynthesis of zinc oxide nanoparticles for biomedicine and environmental applications. Advances in Natural Sciences: Nanoscience and Nanotechnology, 14(4), p.043001.

14. Bhilkar, P., Shrivastav, K., Kahate, A., Triphaty, S., Madankar, R., Chaudhary, A. and Somkuwar, S., 2024. Bioinspired zinc-based nanomaterials: Synthesis, biomedical, environmental and agricultural applications. Materials Research Foundations, pp.81-112.
15. Sundaresan, U. and Kasi, G., 2024. Synthesis of ZnO nanoparticles using Sargassum wightii ethanol extract and their antibacterial and anticancer applications. Biomass Conversion and Biorefinery, 14(20), pp.26173-26191.
16. Adhithi, M., Yogeswari, M., Dhanalakshmi, K., Sangeetha, P., Ehthishamul Haque, M., Sangeetha, B., Sivakumar, S., Bharathi, B.E., 2026. Green-synthesized MgO nanoparticles from Gracilaria folifera: Electrochemical and antidiabetic study. Applied Chemical Engineering, 9(2), pp.1–17.
17. Sivakumar, K., Phycosynthesis of silver nanoparticles from extract of Gracilaria foliifera (Forsskal) Boergesen.
18. Mansour, A.T., Alprol, A.E., Khedawy, M., Abualnaja, K.M., Shalaby, T.A., Rayan, G., Ramadan, K.M. and Ashour, M., 2022. Green synthesis of zinc oxide nanoparticles using red seaweed for the elimination of organic toxic dye from an aqueous solution. Materials, 15(15), p.5169.
19. Chaudhary, R., Nawaz, K., Khan, A.K., Hano, C., Abbasi, B.H. and Anjum, S., 2020. An overview of the algae-mediated biosynthesis of nanoparticles and their biomedical applications. Biomolecules, 10(11), p.1498.
20. Dhinesh, D., Ramanathan, S., Sagar, S. and Jeyaraj, G., 2025. Marine Algae-Derived Nanocomposites for Dual Therapeutic Action: A Green Synthesis Approach to Oral Cancer and Inflammation Control.
21. Anbazhagi, S., Murugesan, A., Muthukrishnan, P., Paramanantham, M., Rajasekar, S., Pazhanisamy, T., Arivazhagan, S. and Karuppiah, C., 2025. Synthesis and characterization of ZnO/MgO nanocomposites: Targeted drug delivery strategies for cancer treatment. Inorganic Chemistry Communications, 180, p.115014.
22. Sharma, S., Yamuna, K.S., Sheeba Rani, S., Sangeetha, B., Sivakumar, S., Bharathi, B.E., Guru Prasad, L., 2025. Synthesis and characterization of aluminum-doped tin oxide nanoparticles for aerospace applications. Digest Journal of Nanomaterials and Biostructures, 20(2), pp.585–594.
23. Hameed, H., Waheed, A., Sharif, M.S., Saleem, M., Afreen, A., Tariq, M., Kamal, A., Al-Onazi, W.A., Al Farraj, D.A., Ahmad, S. and Mahmoud, R.M., 2023. Green synthesis of zinc oxide (ZnO) nanoparticles from green algae and their assessment in various biological applications. Micromachines, 14(5), p.928.
24. Kumar, P., Saravanan, P., Baskar, G., Chitrashalini, S., Omer, S.N., Subashini, S., Rajeshkannan, R. and Venkatkumar, S., 2024. Synthesis and characterization of Ag-decorated ZnO/MgO nanocomposite using a novel phyto-assisted biomimetic approach for anti-microbial and anti-biofilm applications. Inorganic Chemistry Communications, 170, p.113443.
25. Selim, S., Almuhayawi, M.S., Saddiq, A.A., Alruhaili, M.H., Saied, E., Sharaf, M.H., Tarabulsi, M.K. and Al Jaouni, S.K., 2025. Synthesis of novel MgO-ZnO nanocomposite using Pluchea indica leaf extract and study of their biological activities. Bioresources and Bioprocessing, 12(1), p.33.
26. Narm, T.S., Hamidinezhad, H., Sabouri, Z. and Darroudi, M., 2024. Green synthesis of silver doped zinc oxide/magnesium oxide nanocomposite for waste water treatment and examination of their cytotoxicity properties. Heliyon, 10(9).
27. Sivakumar, S., Nagaraj, P., Surendiran, S., Sangeetha, P., Karthikeyan, B., Manikandan, C.T., Balashanmugam, S., Bharathi, B.E., 2026. Aluminium-doped SnO_2 nanoparticles: Synthesis, structural and optical modifications for enhanced photocatalytic environmental applications. AIP Advances, 16(4), p.045124.
28. Ratnam, M.V., Karthikeyan, C., Rao, K.N. and Meena, V., 2020. Magnesium oxide nanoparticles for effective photocatalytic degradation of methyl red dye in aqueous solutions: optimization studies using response surface methodology. Materials Today: Proceedings, 26, pp.2308-2313.
29. Panchal, P., Paul, D.R., Sharma, A., Hooda, D., Yadav, R., Meena, P. and Nehra, S.P., 2019. Phytoextract mediated ZnO/MgO nanocomposites for photocatalytic and antibacterial activities. Journal of Photochemistry and Photobiology A: Chemistry, 385, p.112049.
30. Siddique, A.B., Shaheen, M.A., Abbas, A., Zaman, Y., Bratty, M.A., Najmi, A., Hanbashi, A., Mustaqeem, M., Alhazmi, H.A., ur Rehman, Z. and Zoghebi, K., 2024. Thermodynamic and kinetic insights into azo dyes photocatalytic degradation on biogenically synthesized ZnO nanoparticles and their antibacterial potential. Heliyon, 10(23).
31. Gingașu, D., Mindru, I., Culiță, D.C., Predoană, L., Petcu, G., Ciobanu, M., Preda, S., Pandele-Cușu, J. and Petrescu, S., 2021. MgO obtained by chemical and green synthesis methods and applied in photocatalytic degradation of methyl orange. Rev. Roum. Chim, 66(5), pp.463-473.
32. Ali, M.H., Mahmoud, A., Al-Afify, A.D. and Belal, D.M., 2026. Enhancing Degradation of Methyl Orange Dye Using Green Zinc Oxide Nanoparticles Synthesized with Exopolysaccharides (EPS) Extracted from Cyanobacterial Mats. Water, Air, & Soil Pollution, 237(1), pp.1-19.
33. Shaikh, B., Bhatti, M.A., Shah, A.A., Tahira, A., Shah, A.K., Usto, A., Aftab, U., Bukhari, S.I., Alshehri, S., Shah Bukhari, S.N.U. and Tonezzer, M., 2022. Mn3O4@ ZnO hybrid material: an excellent photocatalyst for the degradation of synthetic dyes including methylene blue, methyl orange and malachite green. Nanomaterials, 12(21), p.3754.
34. Oyewo, O.A., Ramaila, S., Mavuru, L. and Onwudiwe, D.C., 2022. Enhanced photocatalytic degradation of methyl orange using Sn-ZnO/GO nanocomposite. Journal of Photochemistry and Photobiology, 11, p.100131.

35. Velsankar, K., Aravinth, K., Cláudia, P.S.A., Wang, Y., Ameen, F. and Sudhahar, S., 2023. Bio-derived synthesis of MgO nanoparticles and their anticancer and hemolytic bioactivities. Biocatalysis and Agricultural Biotechnology, 53, p.102870.
36. Suba, S., Vijayakumar, S., Vidhya, E., Nilavukkarasi, M., Punitha, V.N. and Prathipkumar, S., 2022. Lactococcus spp., mediated MgO nanoparticles: Assessment of antimicrobial and anticancer activities against intestinal disorder. Results in Chemistry, 4, p.100519.